AIAA JOURNAL
Vol. 35, No. 4, April 1997

Evolution of Vortical Structure over Delta-Wing with Transient Along-Core Blowing

Cheng-Hsiung Kuo,* Ni-Yu Lu,† and Da-Chi Lin†
National Chung Hsing University, Taichung 40227, Taiwan, Republic of China

Over delta-wing with a 75-deg sweep angle and 40-deg of the angle of attack, the vortex core subject to transient along-core blowing is investigated experimentally. In response to the transient along-core blowing, the vortex core, before breakdown, serves as a transmitting vessel that steadily delivers the supplied momentum to overcome the strong adverse along-core pressure gradient, especially near the onset location of the vortex breakdown. The central region of the vortex core is found to be more sensitive to the external perturbation than the outer region. This key characteristic of the vortex core is the reason for transformation of the along-core velocity distribution from the velocity excess (or jet-like) profile to the velocity deficit (or wake-like) profile as the onset of vortex breakdown is encountered. The magnitude of suction peak coefficient measured on the wing surface along the vortex core direction increases in response to the transient along-core blowing. Then it recovers to the unperturbed value as the vortex breakdown recovers to its long-time averaged location. Variation of pressure gradient along the vortex center differs from the gradient of the suction peak coefficient measured on the wing surface along the vortex core direction. The latter is primarily due to the integrated induction from the conical vortex structure above the wing surface. However, the former reflects only the local behavior near the central region of the vortex core.

Nomenclature

A_p	= area of the blowing slot
A_w	= area of the half delta-wing
C	= root chord of the wing (20 cm)
$C_{p,\min}$	= suction peak coefficient, $C_{p,\min} = (p_s - p_\infty)/(1/2\rho U^2)$
C_μ	= blowing coefficient, $C_\mu = (V_p/U_\infty)^2(A_p/A_w)$
Dy	= diameter of the vortex core in spanwise direction in Fig. 3
Dz	= diameter of the vortex core normal to wing surface in Fig. 3
p_c	= pressure at the vortex center
p_s	= pressure measured on the wing surface
R_c	= $(Dy + Dz)/4$
$r*$	= dimensionless radial distance, $r* = r/R_c$
s	= local semi-span at any X/C location
$t*$	= dimensionless time, $t* = tU_\infty/C$
U_∞	= free stream velocity (15 cm/s)
$u*$	= normalized along-core velocity, u/U_∞
u_c*	= normalized centerline velocity, u_c/U_∞
V_p	= velocity at the exit of the blowing slot
$w*$	= normalized swirling velocity, w/U_∞
X, Y, Z	= laboratory coordinate in Fig. 1c
X_b	= instantaneous vortex breakdown location
x, y, z	= coordinate system fixed on the vortex core
$y_{1/2}$	= half-width of the suction peak distribution
α	= angle of attack of the wing
β	= angle of vortex core from the platform
Γ	= circulation
$\Gamma*$	= dimensionless circulation, $\Gamma* = \Gamma/CU_\infty$
θ	= the angle of vortex core above the wing surface
Λ	= sweep angle of the wing

Introduction

IT is well known that the vortex structure over a highly swept delta-wing induces a vortex lift on behalf of the performance of delta-wing especially at high angles of attack (AOA).[1] The supermaneuverability idea[2] for a fighter airplane inspired research on vortex-dominated flow structure in the poststall range of the AOA. It is of central importance to optimally reorganize the unsteady vortex flow and to control the onset location of vortex breakdown for supermaneuverability and agility in the poststall range of the AOA.[3]

The leading-edge vortex core is very sensitive to external disturbances. For example, Lee et al.[4] found that the vortex breakdown location would become very unstable when the freestream turbulence level was around 0.5–1.5%. However, suitable types of time-dependent perturbations applied to the vortex structure over delta-wings create high lift at high AOA. Shi et al.[5] observed qualitatively that a single jet blowing, issued from the wing surface in the flow direction, delayed the onset location of vortex breakdown. They demonstrated that the length of vortex core before breakdown can be effectively enlarged by proper arrangement of blowing in location and in orientation. Reynolds and Abtahi[6] described that upstream propagation of vortex breakdown is closely related to the motion of nonlinear solitary waves. Finally, a wave-block concept was suggested to control the onset location of vortex breakdown. In the range of high-speed experiments ($M = 0.35$ and 0.7) in the wind tunnel, Bradley et al.[7] and Campbell[8] find a large increase in lift at high AOA as the vortex core is perturbed by spanwise blowing.

For periodic perturbations in the direction tangent to the leading edge, Gu et al.[9] reported the onset location of vortex breakdown as a strong function of perturbation periods. In their results, the most effective period of the alternate suction-blowing perturbation was about one convective time scale C/U_∞. When perturbed at this efficient period, the vortical structure over the delta-wing is reorganized and the onset location of vortex breakdown is substantially delayed. Recently, Kuo and Lu[10] also explored nearly the same effective time scale when a small amount of the along-core blowing perturbation was issued harmonically from the wing apex.

Although the effectiveness of these blowing techniques was found to be a strong function of the AOA, the sweep angle, the perturbation amplitude, and the leading-edge geometry (either sharp or blunt),[5,7–10] the detailed characteristics of the vortex core in response to transient blowing are not yet complete. Consequently, the objective of this study is to investigate the characteristics of the vortex core (including spatial distribution and time-dependent evolution) over a highly swept delta-wing at high AOA in response to the transient along-core blowing issued from the wing apex. Moreover, the pressure gradient along the centerline of the vortex core is

Received July 22, 1996; revision received Nov. 26, 1996; accepted for publication Dec. 6, 1996.

*Associate Professor, Department of Mechanical Engineering.
†Graduate Student, Department of Mechanical Engineering.

addressed in comparison with that measured on the leeward wing surface along the vortex core direction.

Facilities and Experimental Setup

Experimental Conditions and Model Arrangement

All experiments were carried out in a low-speed recirculation water channel. The turbulence intensity was reduced to a level of 0.42% at $Re_C = 3.06 \times 10^4$. Moreover, the nonuniformity of freestream velocity distribution was around 1.2%. The momentum coefficient of the along-core blowing is defined as $C_\mu = (V_p/U_\infty)^2(A_p/A_w)$. For this definition, both V_p and U_∞ denote the measured velocity issuing from the blowing slot and the freestream velocity. Moreover, A_p and A_w denote the areas of the blowing slot and of the wing, respectively. In the present study, the blowing slot has a diameter of 0.5 mm and the momentum coefficient is selected to be 0.088. The transient along-core blowing is in the form of a finite impulse lasting for $0.6\,C/U_\infty$ and then it suddenly terminates.

The half delta-wing, with a 75-deg sweep angle, was beveled upward at an angle of 25 deg, forming a sharp leading edge. As shown in Fig. 1a, the model of the half delta-wing was set on the platform having a leading edge of a 5:1 elliptic profile. The combination of the half delta-wing and the platform indeed simulated the actual wing–fuselage arrangement. The fully spanned platform was placed horizontally about 5 cm above the bottom of the channel, allowing uniform inflow with zero incidence angle relative to the platform. Moreover, although the half delta-wing was installed on the platform, the blockage ratio was around 0.028 at AOA = 40 deg. Figures 1a and 1b show the use of the rotating circular disk to align the along-core blowing direction with the axis of the primary vortex core.

With the wing apex as the origin, the coordinate system is defined in Fig. 1c. The positive x and y denote the directions along and normal to the axis of the primary vortex core, respectively. However, X/C denotes the streamwise distance measured from the origin (or the wing apex) as a fraction of the root chord C. The direction of positive z denotes the distance away from the wing surface, and s represents the local semispan at any X/C locations.

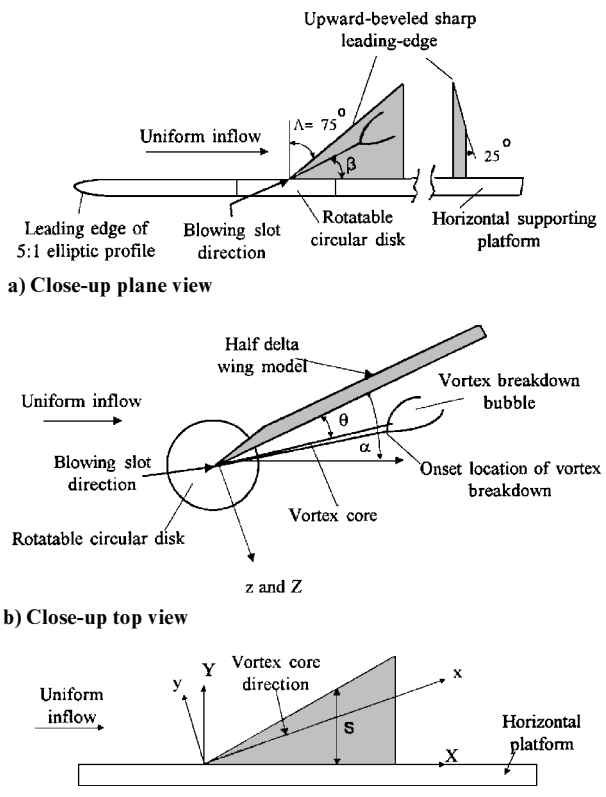

Fig. 1 Arrangements and installation of the half delta-wing model on the fully spanned horizontal platform.

Experimental Technique

The phase-trigger technique initiates the data acquisition at the onset instant of transient along-core blowing. It provides the same initial instant for all the velocity measurements within the flow domain. This technique allows conversion of the point-by-point velocity measurements at different times into the instantaneous spatial velocity distributions. This conversion, starting from the onset instant of transient along-core blowing, allows elucidation of the time-dependent evolution of the flow structure and exploration of some important nature of the vortex core. This technique was also applied to the acquisition of the surface pressure time signals when subject to the transient along-core blowing. For detailed information about the alignment and adjustments of the along-core blowing direction as well as the personal-computer-based blowing control device, refer to Kuo and Lu[10] and Kuo and Lin.[11]

Velocity and Surface Pressure Measurements

The whole field measurements of the along-core velocity were performed by the nonintrusive LDA system on the cross-flow planes ranging from $X/C = 0.3$ to 0.7. Under the specified flow and the blowing conditions, the planes were selected so that the upstream movement of the vortex breakdown could be observed within $0.3 < X/C < 0.7$ during the evolutionary process. Depending on the size of the vortex core at different X/C locations, the number of measuring points on each plane ranges from 380 to 620 points to provide good spatial resolution. The positioning of each measuring point was controlled by a precise traversing table of 0.01-mm accuracy. (The instantaneous circulation of the vortex core was evaluated by line integration around the region enclosed by the closed curve B shown later in the inset of Fig. 10.) Furthermore, the average size of the seeding particles (TiO_2) was about 8 μm. The responding time of the seeding particles relative to the fluid motion was estimated to be around 6.2 μs. The fast responding time, together with small size and high density, of the seeding particles further ensured the continuous and reliable velocity time signals acquired from the laser Doppler anemometer system.

Surface-pressure measurements were carried out along the vortex core direction at various X/C locations on the leeward wing surface. The vortex core direction on the wing surface was predetermined by flow visualization of food-color dye released from the wing apex. A series of pressure taps (0.5 mm in diameter) was drilled on the leeward wing surface along the predetermined vortex core direction at six X/C locations shown in Fig. 2. The pressure-transmitting tubes were buried inside the wing thickness having its outlet connector at the trailing edge of the wing. A thick-walled tygon tube was selected to connect the pressure transducer with the outlet connector from which the pressure signal is transmitted. A minimum length of the tygon tube is required to avoid too much decay before the pressure signal is sensed by the pressure transducer. Nevertheless, the transducer had a rising time of 0.003 s. Therefore, the sampling time interval of 0.01 s is long enough to accurately obtain reliable time signals of the surface pressure.

Data Reduction Process

At each measuring location within the flow domain, the time signals were taken for 10 sample experiments by a phase-trigger technique. The time signals at each y/s location (shown later in

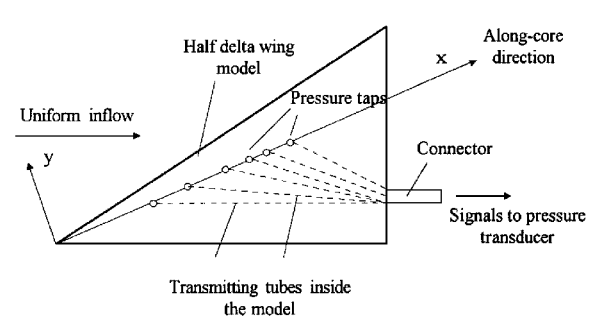

Fig. 2 Sketch of the device for surface-pressure measurements. Pressure taps are located on the wing surface along the vortex core direction at X/C = 0.3, 0.4, 0.5, 0.55, 0.6, and 0.7.

Figs. 6 and 7) were obtained by ensemble averaging the phase-triggered time signals of the 10 sample runs at that specified location. Collections of the ensemble-averaged time signals at all measuring points within the flow domain for the same instant will yield the instantaneous cross-flow velocity profile, as shown in Fig. 3 and, later, in Fig. 5.

Results and Discussions

Basic Flow Structure of Leading-Edge Vortex

In Fig. 3, the abscissa shows the typical prebreakdown dimensionless velocity distributions, normalized by the freestream velocity U_∞ of both the along-core $u*$ and the swirling $w*$ components across the vortex core at $X/C = 0.3$ and $t* = 2.7$. Before the vortex breakdown occurs, the along-core velocity distribution across the vortex core exhibits an excess velocity (or jet-like) profile with maximum overshoot of $1.8\,U_\infty$. The position of maximum overshoot indicates approximately the center location of the vortex core at that specific X/C location. The magnitude of the along-core velocity component approaches the freestream velocity near the local leading edge ($y/s = 1.0$). On the other hand, the magnitude becomes nearly zero to satisfy the no-slip condition on the horizontal platform as y/s approaches zero. Obviously, within $0.4 < y/s < 0.7$, the symmetric along-core velocity distribution about the vortex center ensures the axisymmetric structure of the vortex core. The swirling velocity distribution across the vortex core closely resembles the Berger vortex, with the highest velocity gradient near the vortex center.[12] Considering an idealized point vortex, the location corresponding to zero swirling velocity represents the center of the vortex core. In this experiment, the center of the leading-edge vortex was around $z/s = 0.6$ (as indicated by $*$ in Fig. 3) above the wing surface.

Vortex Breakdown Recovery After Transient Along-Core Blowing

When subject to transient along-core blowing issued from the wing apex, Fig. 4 shows the instantaneous onset location of vortex breakdown X_b/C for some selected runs of 10 sample runs. The

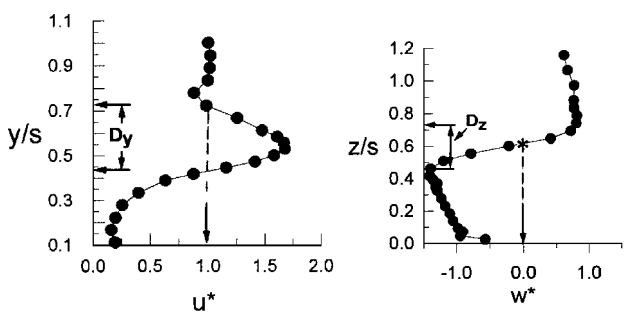

Fig. 3 Typical prebreakdown distribution of the along-core and swirling velocity components across the vortex core at $X/C = 0.3$ and 40 deg of the angle of attack. Both are normalized by the freestream velocity. s is the local semispan.

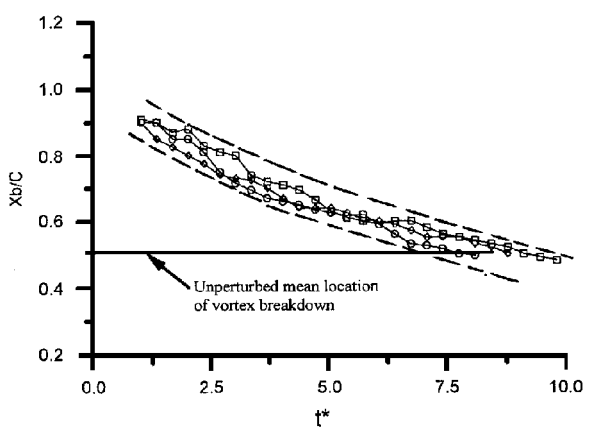

Fig. 4 Instantaneous onset location of vortex breakdown subject to the transient along-core blowing issued from the wing apex. The band between two dashed lines represents 99% confidence interval among the data points: $\alpha = 40$-deg, $C_\mu = 0.088$, and $\Lambda = 75$-deg.

abscissa denotes the dimensionless time $t* = tU_\infty/C$ that begins from the onset of transient blowing. Moreover, the band bounded between two dashed lines indicates the 99% confidence interval among the 10 sample runs, giving the maximum deviation about $0.08C$. This deviation includes the $0.05C$ error caused by the unsteady nature of the vortex breakdown location in the unperturbed case. The horizontal solid line at $X_{b/C} = 0.5$ indicates the long-time averaged onset location of vortex breakdown without blowing.

In Fig. 4 between $t* = 0$ and $t* = 1.2$, the exact location of vortex breakdown can hardly be identified because of quick diffusion of the food-colored dye carried by the high-velocity blowing stream. Therefore, no data points are available for $t* < 1.2$ in Fig. 4. However, the farthest visible location of vortex breakdown greatly exceeds the horizontal solid-line level, indicating substantial delay of the onset location of vortex breakdown. This delay of vortex breakdown is supported by the theoretical predictions.[13,14] After transient along-core blowing, the onset location of vortex breakdown recovered monotonously from the farthest visible location toward the unperturbed level (solid-line level) as time continued. The overall recovering process took about 6.8–8.8 times the convection time scale C/U_∞ to reach the solid-line level.

Evolution of the Vortex Structure After Transient Along-Core Blowing

Instantaneous cross-flow distributions of the along-core velocity at successive X/C locations are shown in Fig. 5 for various instants during the evolutionary process. Up to $t* = 2.7$, all the along-core velocity distributions across the vortex core showed a unique jet-like pattern with a maximum value of overshoot near $y/s = 0.54$–0.62 at successive X/C locations. Referring to the instantaneous breakdown location of the leading-edge vortex core shown in Fig. 4, the onset location of the vortex breakdown has been delayed beyond $X/C = 0.7$ at $t* = 2.7$. Therefore, the unique jet-like pattern of the along-core velocity ensures that there is no indication of the onset of vortex breakdown within $X/C = 0.3$ and 0.7.

As time proceeded to $t* = 4.05$, the jet-like profiles of the along-core velocity across the vortex core extended up to $X/C = 0.55$. Beyond this location, the central portion of the jet-like profile was flattened first at $X/C = 0.65$; meanwhile, it became irregular at $X/C = 0.7$, indicating the onset of vortex breakdown. Subsequently, at $t* = 6.75$, the cross-flow distributions of the along-core velocity at $X/C = 0.65$ and 0.7 became a velocity deficit (or wake-like) profile. Not until $t* = 9.45$ did the onset location of vortex breakdown almost recover to the unperturbed position $X/C = 0.5$ (that is, the solid line level shown in Fig. 4). At this moment, the irregular cross-flow distributions $u*(y)$ at both $X/C = 0.5$ and 0.55 locations were the results of the unsteady nature (back-and-forth movement) of the vortex breakdown location. Throughout the evolutionary process, it is clear that the jet-like cross-flow distributions of the along-core velocity at any X/C location first become distorted while the vortex breakdown approaches. Then, it transforms into the wake-like pattern as the onset location of vortex breakdown has passed through this specified location.

Prebreakdown Vortex Characteristics After Transient Along-Core Blowing

The instantaneous cross-flow distribution of the along-core velocity and its streamwise variations are depicted in Fig. 5. It illustrates the global evolution of the vortex core in terms of the jet-like and the wake-like profiles of the along-core velocity. However, details of the characteristics of the vortex core should be extracted from the velocity time signals to gain insight into the flow characteristics of the vortex structure.

Referring to the case without blowing, the mean onset location of vortex breakdown occurred near $X/C = 0.5$. In Fig. 6, the along-core velocity time signals in response to the transient along-core blowing were taken at various spanwise locations (y/s) across the vortex core on the cross-sectional plane at $X/C = 0.3$. Before the blowing reached the $X/C = 0.3$ location, the initial state of the vortex core (as the horizontal arrows at $t* = 0$ at different y/s locations) showed higher along-core velocity at the vortex center and lower along-core velocity outside the vortex core. This distribution resembles the jet-like profile and further confirms the initial unburst

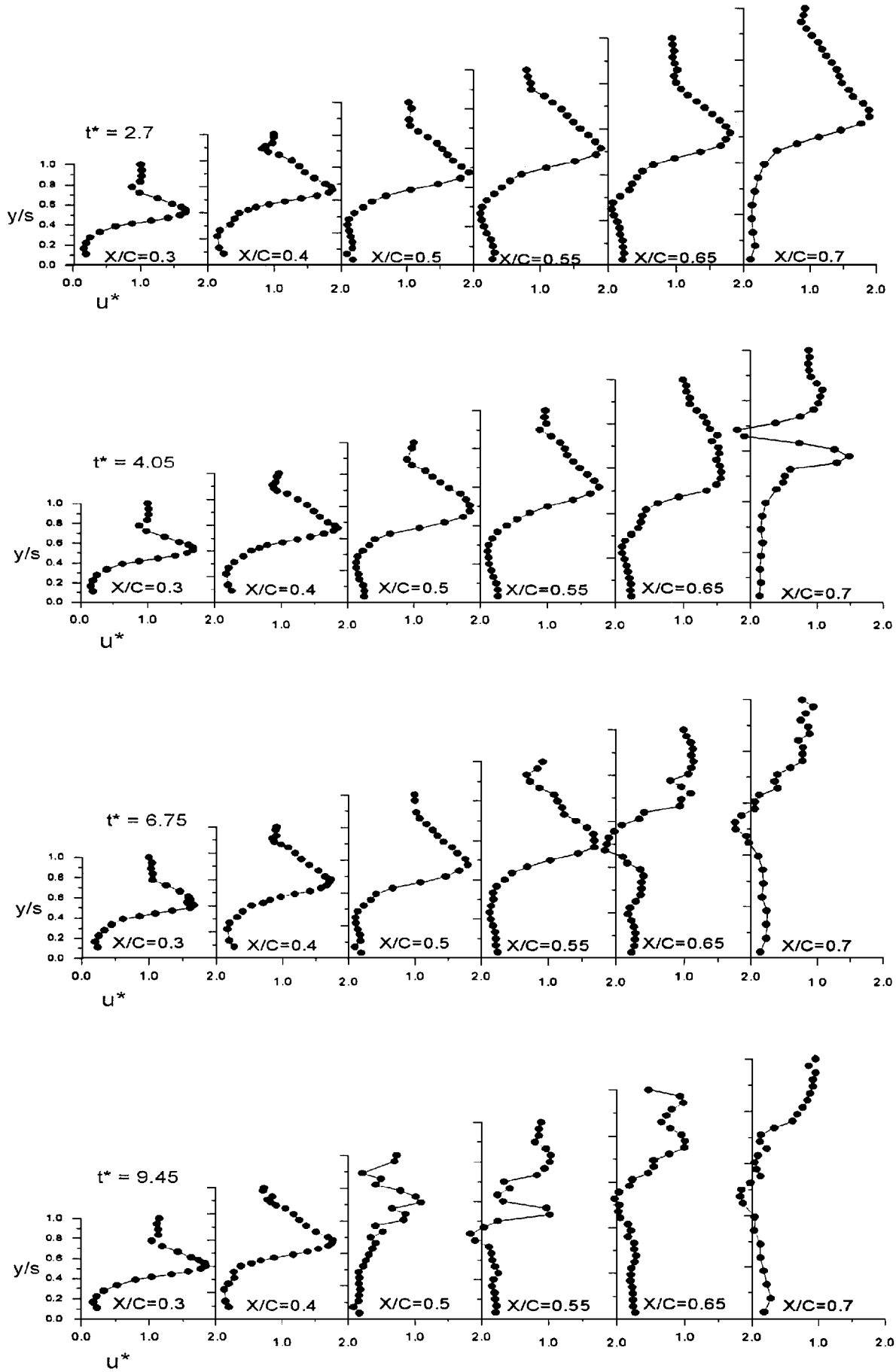

Fig. 5 Instantaneous spatial distribution of the along-core velocity across the vortex core at successive *X/C* locations. Transformation of the jet-like profiles to the wake-like profiles are shown as the onset location of vortex breakdown propagates upstream. Before vortex breakdown, the along-core velocity distributions exhibit jet-like profiles; after breakdown, the wake-like profiles are presented.

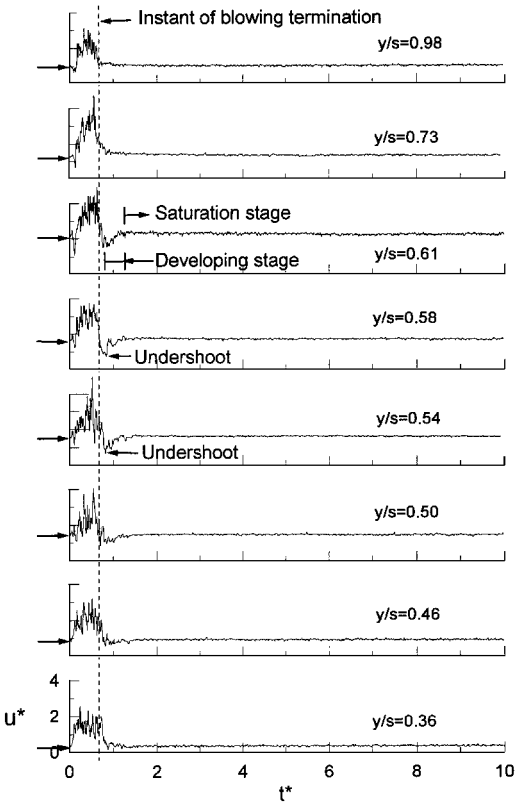

Fig. 6 Time signals of along-core velocity at various *y/s* locations at *X/C* = 0.3; *u*∗= normalized along-core velocity, and *t*∗= dimensionless time. Ordinates are the same scale. Horizontal arrows at *t*∗= 0 indicate initial stage of the vortex core at different *y/s* locations.

(or prebreakdown) state at $X/C = 0.3$. In response to the transient along-core blowing, the magnitude of the along-core velocity increased drastically by adding the linear along-core momentum into the vortex core. Then it decreased rather rapidly as the transient along-core blowing suddenly terminated.

Within the central region of the vortex core (i.e., $0.54 < y/s < 0.61$ in Fig. 6), the time signal decreased drastically to a minimum, forming an undershoot in response to the sudden termination of the along-core blowing. Then the vortex core experienced the developing stage by increasing the magnitude from the undershoot. Eventually, the time signal reached the initial state level and remained constant as time proceeded. Outside this region, the time signal decreased and settled down to the initial state level in a monotonous way. At $t* > 2$, the magnitudes of the along-core velocity across the vortex core recovered to their initial values and remained nearly unchanged as time continued. This implies that the vortex core, before vortex breakdown, serves only as a transmitting vessel that steadily delivers the linear momentum supplied by transient along-core blowing.

Along-Core Sensitivity of the Vortex Core

Close examination of the time signals in Fig. 6 reveals that the along-core velocity time signals exhibit different forms to relax to their initial values at different y/s locations after the transient along-core blowing terminates suddenly.

Previous investigations indicated that there exists a velocity oscillation within the vortex breakdown bubble.[12] Moreover, the frequency-dependent amplitude response (or the amount of the delay) induced by harmonic excitation has a maximum near the frequency in resonance with some characteristic frequency.[9,11] This response resembles that of the simplified second-order oscillatory system. Based on the features mentioned earlier, the dynamic characteristics of the vortex core in response to the transient along-core blowing may be described by the lumped mass-damper-spring system. The governing equation can be expressed as

$$(1/\omega_n^2)\ddot{x} + (2\xi/\omega_n)\dot{x} + x = 0 \qquad (1)$$

In Eq. (1),

$$\xi = c/2\sqrt{km}$$

represents the dimensionless damping coefficient and $\omega_n = \sqrt{(k/m)}$ denotes the natural frequency of the vortex system. Nevertheless, m is the mass within the vortex core, c corresponds to the viscous damping, and k denotes the axial stiffness of the vortex core before the vortex breaks down.

Within the central region of the vortex core, the time traces shown in Fig. 6 exhibit undershoot characteristics while the transient along-core blowing terminates suddenly. The characteristic of undershoot behavior suggests that the inertia term be important in Eq. (1), implying small ω_n. Within the central region of the vortex core, a small value of ω_n will lead to small along-core stiffness k if the mass of the vortex core is assumed to be constant.

On the other hand, within the outer region of the vortex core, the time traces in Fig. 6 vary monotonously in response to the blowing termination. This characteristic clearly suggests that the second term in Eq. (1) be dominant and the inertia term be negligible because of the relatively large ω_n. Thus, the governing differential equation is degraded into a lumped first-order system:

$$(2\xi/\omega_n)\dot{x} + x = 0 \qquad (2)$$

In this situation, large ω_n implies a higher value of the along-core stiffness k and a smaller value of the time constant $\tau = 2\xi/\omega_n$ in Eq. (2).

In other words, the vortex core is relatively insensitive to the external perturbation because of high along-core stiffness within the outer region. Furthermore, it settles down to the initial state more quickly after termination of the along-core blowing because of a small time constant. However, the characteristic of low along-core stiffness makes the central region of the vortex core very sensitive to sudden termination of the along-core blowing. Because of the quite different along-core stiffness of the vortex core, the along-core velocity within the central region of the vortex core experiences significant change while vortex breakdown approaches. However, the along-core velocity within the outer region exhibits only a small change.

Postbreakdown Vortex Characteristics After Transient Along-Core Blowing

In response to the transient along-core blowing, Fig. 7 shows the along-core velocity time signals across the vortex core at the $X/C = 0.5$ location. During blowing and immediately after sudden termination of blowing, characteristics of the vortex core similar to those in Fig. 6 can also be found. As indicated by the horizontal arrows at $t* = 0$ in Fig. 7, the initial state of the vortex core has an irregular cross-flow distribution $u*(y)$. This distribution clearly indicates the breakdown of the vortex core at the $X/C = 0.5$ location.

Within the central region of the vortex core (i.e., $y/s = 0.54$–0.64 in Fig. 7), the along-core velocity increases during the developing stage. The magnitude of $u*$ reaches a plateau region termed the saturation stage. However, within the outer region ($y/s = 0.75$–0.9 and 0.45 in Fig. 7) of the vortex core, the magnitude of the along-core velocity decreases slowly toward the initial state.

The saturation stage spans about $6.8C/U_\infty$. During this stage, the along-core velocity near the central region ($0.54 < y/s < 0.64$ in Fig. 7) is higher than that in the outer region of the vortex core, leading to a similar profile to the jet-like distribution in Fig. 5 (for example, at $X/C = 0.5$ and $t* = 4.05$). During the developing and saturation stages, transformation of the initially broken-down state to the jet-like velocity profile across the vortex core implies that the vortex core has been reorganized. This reorganization of the vortex core clearly suggests that the momentum, supplied by the transient along-core blowing, is used primarily to increase the along-core momentum and to overcome the strong adverse along-core pressure gradient near the location of vortex breakdown. As a result, the onset location of the vortex breakdown can be effectively delayed further downstream.

In the decaying stage of Fig. 7, the magnitude of the along-core velocity within the central region of the vortex core dropped suddenly in a very short time. Not until $t* = 9.45$ was small or negative

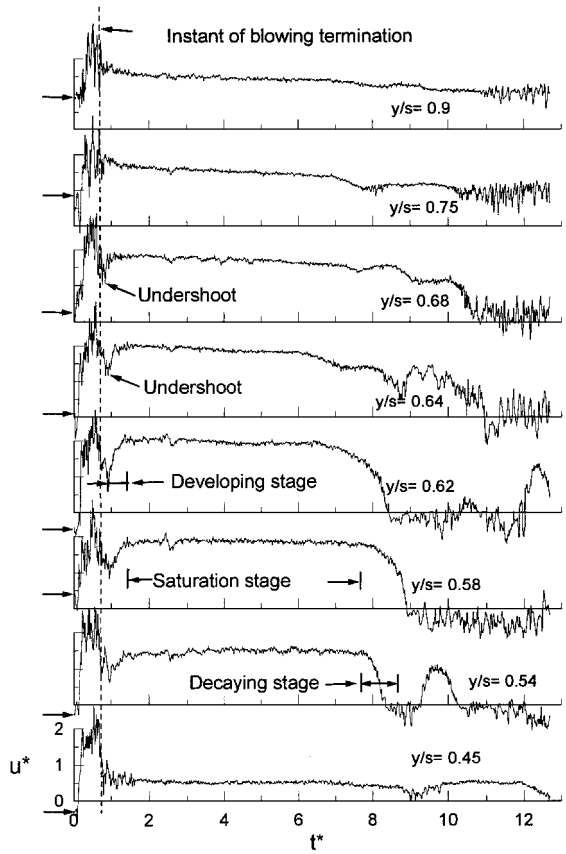

Fig. 7 Time signals of the along-core velocity at various *y/s* locations at *X/C* = 0.5; *u= normalized along-core velocity and *t**= dimensionless time. Ordinates are the same scale. Horizontal arrows at *t**= 0 indicate initial stage of the vortex core at different *y/s* locations.**

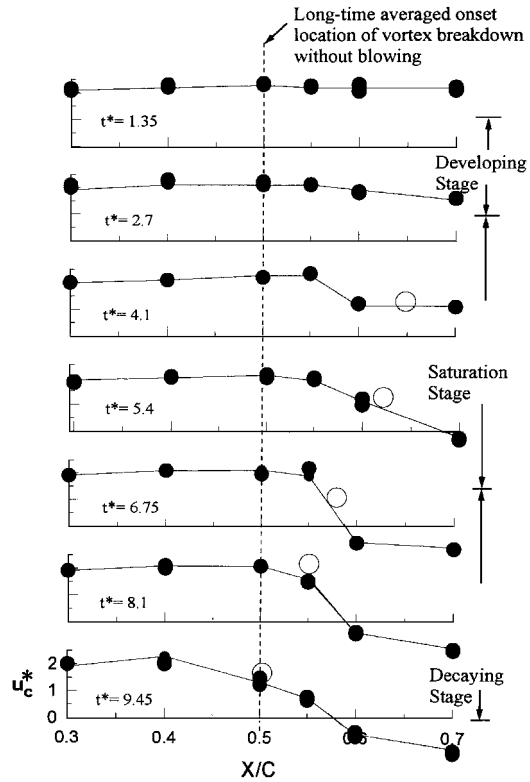

Fig. 8 Streamwise variations of the normalized centerline velocity of the vortex core at different instants during recovery of the vortex breakdown location. Ordinates are the same scale. Solid lines represent mean trend of variation. Maximum deviation is no more than 2.35% of the freestream velocity. Open circles on each curve indicate instantaneous locations of vortex breakdown.

along-core velocity found in the central region of vortex core. However, higher and positive along-core velocity was detected in the outer region of the vortex core. This wake-like along-core velocity profile clearly indicates the already broken-down state of the vortex core at $X/C = 0.5$ and $t* > 9.45$.

The coincidence of the sudden drop of the along-core velocity around $t* = 9.45$ in Fig. 7 with the irregular velocity profile in Fig. 5 at $t* = 9.45$ strongly suggests that this sudden drop is primarily caused by the onset of vortex breakdown at $X/C = 0.5$. Around $t* = 9.45$ in Fig. 7, the along-core velocity drops suddenly within the central region of the vortex core. However, it changes promptly but only mildly in the outer region. This evidence strongly shows the highly sensitive characteristic within the central region of the vortex core. As shown in Figs. 6 and 7, the quite different along-core sensitivity of the central and outer regions of the vortex core before breakdown is an important characteristic for the vortex-dominated flow structure over delta-wing. Obviously, this key characteristic is a reason for transformation of the along-core velocity distribution from the jet-like profile to the wake-like profile when the onset location of vortex breakdown approaches.

Pressure Distribution Along the Vortex Center

Figure 8 shows the streamwise distributions of centerline velocity u_c^* normalized by the freestream velocity at different instants after termination of the transient along-core blowing. Before the along-core blowing was applied, the mean location of vortex breakdown occurred near $X/C = 0.5$ (vertical dashed line in Fig. 8). At $t* = 1.35$ during the developing stage, the along-core velocity at the vortex center remained nearly constant in the streamwise direction. During the saturation stage ($t* = 4.1$ in Fig. 8), the descending variation of u_c^* in the streamwise direction between $X/C = 0.55$ and 0.7 roughly corresponded to the onset location of vortex breakdown at this instant. As time continued to $t* = 5.4$, the descending part moved progressively upstream. This upstream movement of vortex breakdown location kept pace with the instantaneous location of vortex breakdown (i.e., the open circle on each curve in Fig. 8). Before the vortex broke down, the results in Figs. 6–8 further suggest that the along-core velocity at the vortex center not only remained constant in time but also remained almost unchanged in the streamwise direction.

Considering the cylindrical, axisymmetric assumptions of the vortex core before breakdown, the simplified dimensionless axial momentum equation in the polar coordinate evaluated at the vortex center ($r = 0$) can be expressed as

$$\left(\frac{\partial u*}{\partial t*} + u*\frac{\partial u*}{\partial x*}\right)\bigg|_{r=0} = -2\frac{\partial C_p}{\partial x*}\bigg|_{r=0} + \frac{1}{Re_C}\left[\left(\frac{C}{R_c}\right)^2 \frac{\partial^2 u*}{\partial r*^2}\right]\bigg|_{r=0} \tag{3}$$

Therefore, the pressure gradient along the vortex center can be estimated by the sum of the convective term, the local rate of change of the axial velocity at vortex center, and the term $(C/R_c)^2(\partial^2 u*/\partial r*^2)(1/Re_C)|_{r=0}$.

In the developing stage, both $\partial u_c^*/\partial t* > 0$ in Figs. 6 and 7 and $\partial u_c^*/\partial x* \approx 0$ in Fig. 8 clearly indicate a strong favorable pressure gradient along the vortex center. During the saturation stage, the magnitude of $\partial u_c^*/\partial x*$ in Fig. 8 is slightly positive within $0.3 < X/C < 0.5$. The term $\partial u_c^*/\partial t*$ in Figs. 6 and 7 at the vortex center is nearly zero. Furthermore, before vortex breakdown, the jet-like profile of the along-core velocity always gives $\partial^2 u_c^*/\partial r*^2|_{r=0} < 0$ during the developing and the saturation stages. As a consequence, the sum of these three terms clearly indicates the strong favorable pressure gradient along the vortex center. However, during the saturation stage and beyond the $X/C = 0.5$ location, the sum of $\partial u_c^*/\partial x* < 0$ in Fig. 8, $\partial u_c/\partial t* \approx 0$ in Fig. 7, and $\partial^2 u_c^*/\partial r*^2|_{r=0} < 0$ clearly indicates the existence of the mild adverse along-core pressure gradient.

During the decaying stage and $X/C < 0.5$, $\partial u_c/\partial t* \approx 0$ in Fig. 6, and $\partial u_c^*/\partial x* \approx 0$ in Fig. 8, along with $\partial^2 u_c^*/\partial r*^2|_{r=0} < 0$ for the

jet-like profile, lead to the overall mild favorable along-core pressure gradient. However, the sums of $\partial u_c^*/\partial x^* < 0$ in Fig. 8, $\partial u_c^*/\partial t^* < 0$ in Fig. 7, and $\partial^2 u_c^*/\partial r^{*2}|_{r=0} > 0$ for the wake-like profile denote the existence of a strong adverse pressure gradient along the vortex center in the region $X/C > 0.5$.

Because the long-time averaged location of vortex breakdown occurs near $X/C = 0.5$ in the case of no blowing, the along-core pressure gradient is always favorable at the vortex center for $X/C < 0.5$. However, for $X/C > 0.5$, the along-core pressure gradient $\partial p_c/\partial x$ varies from a favorable value to an adverse one during the evolutionary process. After the decaying stage at large t^*, the onset location of vortex breakdown almost recovers to the $X/C = 0.5$ location. In this limit, the variation of the pressure gradient along the vortex center $\partial p_c/\partial x$ shown in the rightmost column of Table 1 is similar to that predicted numerically by Robinson et al.[15] over a static delta-wing without blowing. This means that the qualitative estimation of the along-core pressure gradient at the vortex center based on Eq. (3) is a reasonable approach.

Suction Peak Coefficient Variation Along the Vortex Core Direction

The suction peak coefficient $-C_{p,\min}$ measured on the wing surface along the vortex core direction is depicted in Fig. 9 for various instants during the evolutionary process. Obviously, all the curves in Fig. 9 have negative slopes, implying an adverse pressure gradient on the leeward surface along the vortex core direction. As evidenced in Fig. 9, the magnitude of the suction peak coefficient $-C_{p,\min}$ becomes more positive during the developing stage (for example, $t^* < 2.4$). During the saturation and decaying stages, the suction peak coefficient $-C_{p,\min}$ decreases in magnitude. Finally, at $t^* = 12$, the distribution of the suction peak coefficient on the wing surface along the vortex core direction recovers to the case of no blowing. Although the measured value of $-C_{p,\min}$ at $t^* = 12$ is somewhat different from that measured by Roos and Kegelman[16] because of a different sweep angle and AOA, the distribution and the trend are similar. However, in Table 1, the streamwise variations of the $\partial p_c/\partial x$ and the $\partial p_s/\partial x$ are quite different.

Considering the cylindrical, axisymmetric assumption of the vortex core before breakdown, the pressure difference at vortex center

Table 1 Comparison of $\partial p_c/\partial x$ and $\partial p_s/\partial x$ during evolutionary stages[a]

	Developing stage	Saturation stage	Decaying stage
$X/C < 0.5$	$\partial p_c/\partial x < 0$	$\partial p_c/\partial x < 0$	$\partial p_c/\partial x < 0$
	$\partial p_s/\partial x > 0$	$\partial p_s/\partial x > 0$	$\partial p_s/\partial x > 0$
$X/C > 0.5$	$\partial p_c/\partial x < 0$	$\partial p_c/\partial x > 0$ (mild)	$\partial p_c/\partial x > 0$ (strong)
	$\partial p_s/\partial x > 0$	$\partial p_s/\partial x > 0$	$\partial p_s/\partial x > 0$

[a] $\partial p_s/\partial x$ is obtained from Fig. 9. $\partial p_c/\partial x$ is estimated from Figs. 6–8. $X/C = 0.5$ represents long-time averaged onset location of vortex breakdown.

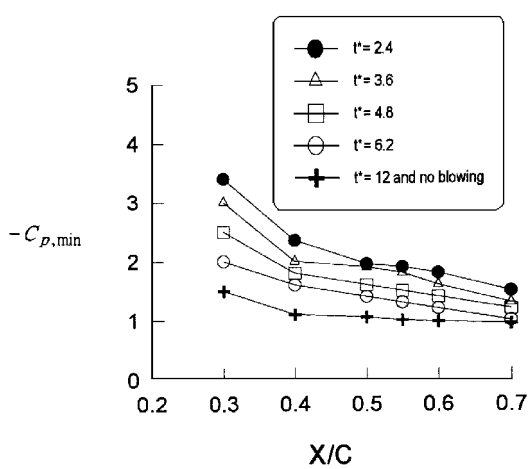

Fig. 9 Suction peak coefficient $-C_{p,\min}$, measured along the vortex core at different instants during evolution of the vortex structure when subject to transient along-core blowing. Maximum deviation of measured coefficient among the sampled data is around 0.035.

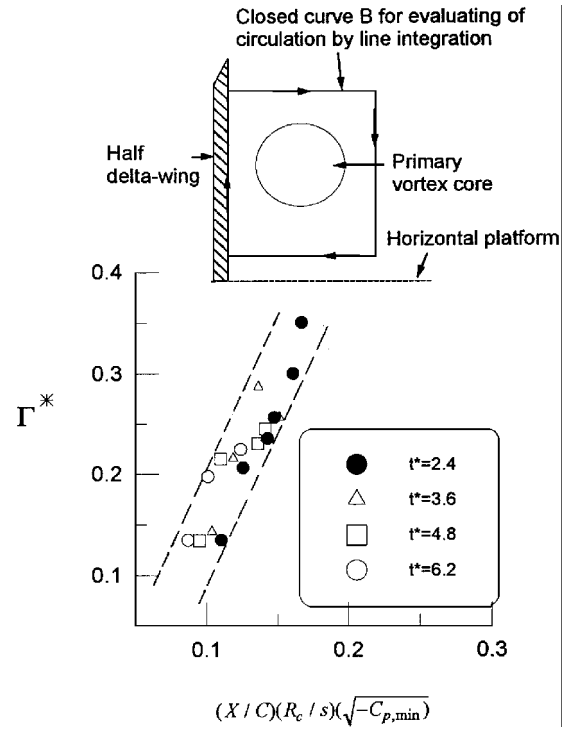

Fig. 10 Dimensionless circulation in relation to $(X/C)(R_c/s)\sqrt{-C_{p,\min}}$ for various instants during evolution of the vortex structure over delta-wing subject to transient along-core blowing. The band between two dashed lines denotes 99% confidence interval of the sample data.

and on the wing surface can be estimated by the simplified radial momentum equation

$$p_s - p_c = \int_0^{Rs} \frac{\rho w^2}{r}\,\mathrm{d}r \tag{4}$$

This equation further indicates that the $\partial p_s/\partial x$ and the $\partial p_c/\partial x$ are different. The difference equals the streamwise gradient of the integrated centrifugal effect due to the swirling velocity around the vortex core. Similarly, in Greenwell and Wood's model[17] $\Gamma^* = (X/C)(y_{1/2}/s)\sqrt{-C_{p,\min}}$, the suction peak measured on the wing surface is also based on the overall induction of a point vortex located above the wing surface.

As suggested by Greenwell and Wood[17] at small AOA, Fig. 10 shows the relationship of

$$\Gamma^* = \Gamma/CU_\infty \quad \text{vs} \quad (X/C)(R_c/s)\sqrt{-C_{p,\min}}$$

Despite the experimental data scattered at different instants during evolution of the vortex core, they all collapse into the band of the 99% confidence interval. In Fig. 10, the general trend of the dimensionless circulation increases with increasing $(X/C)(R_c/s)\sqrt{-C_{p,\min}}$ at poststall AOA.

Both the relations in Eq. (4) and the linear variation in Fig. 10 further point out that the surface pressure gradient along the vortex core direction differs from the along-core pressure gradient at the vortex center. The former is caused primarily by the global induction from the vortex core above the wing. However, the latter represents only local behavior near the central region of the vortex core.

Concluding Remarks

Over delta-wing with a 75-deg sweep angle and 40 deg of the AOA, the vortex core subject to the transient along-core blowing was investigated experimentally. In response to the transient along-core blowing, the vortex core, before vortex breakdown, served as a transmitting vessel that steadily delivered the supplied momentum to overcome the strong adverse along-core pressure gradient, especially near the onset location of the vortex breakdown. The central region of the vortex core was found to be more sensitive than the outer region to external perturbation. This key characteristic was

the reason for transformation of the along-core velocity distribution from the jet-like profile to wake-like profile as the onset of vortex breakdown was encountered. The finding of this characteristic of the vortex core was important and helpful in determining the orientation and locations in the active control applications. In the present study, the substantial delay and the relatively long time of recovery of the vortex breakdown were caused by the along-core blowing and high sensitivity of the central region of the vortex core. Moreover, the magnitude of the suction peak coefficient measured on the wing surface along the vortex core direction increased in response to transient along-core blowing. Then, it recovered to the unperturbed value as the vortex breakdown recovered to its long-time averaged location at $X/C = 0.5$. Variation of pressure gradient along the vortex center differed from that of suction peak coefficient measured on the wing surface along the vortex core direction. The latter is primarily due to the integrated induction from the conical vortex structure above the wing surface. However, the former reflects only the local behavior near the central region of the vortex core.

Acknowledgment

The authors are grateful for support by the National Science Foundation of the Republic of China under Grant NSC-83-0424-E-005-006.

References

[1]Polhamous, E. C., "Predictions of Vortex Lift Characteristics by a Leading-Edge Suction Analogy," *Journal of Aircraft*, Vol. 8, No. 4, 1971, pp. 193–199.

[2]Cord, T. T., and Suchomel, C. F., "Supermaneuverability," AIAA Paper 84-2386, Jan. 1984.

[3]Herbst, W. B., "Future Fighter Technologies," *Journal of Aircraft*, Vol. 17, No. 8, 1980, pp. 561–566.

[4]Lee, M., Shih, C., and Ho, C. M., "Response of a Delta-Wing in Steady and Unsteady Flows," *Proceedings of the Forum on Unsteady Flow Separation*, FED Vol. 52, American Society of Mechanical Engineers, New York, 1987, pp. 19–24.

[5]Shi, Z., Wu, J. M., and Vakili, A. D., "An Investigation of Leading-Edge Vortices on Delta-Wing with Jet Blowing," AIAA Paper 88-0504, Jan. 1988.

[6]Reynolds, G. A., and Abtahi, A. A., "Three Dimensional Vortex Development, Breakdown and Control," AIAA Paper 89-0988, March 1989.

[7]Bradley, R. G., Whitten, P. D., and Wray, W. O., "Leading-Edge Vortex Augmentation in Compressible Flow," *Journal of Aircraft*, Vol. 13, No. 9, 1976, pp. 238–242.

[8]Campbell, J. F., "Augmentation of Vortex Lift by Spanwise Blowing," *Journal of Aircraft*, Vol. 13, No. 9, 1976, pp. 727–732.

[9]Gu, W., Robinson, O., and Rockwell, D., "Control of Vortices on a Delta-Wing by Leading-Edge Injection," *AIAA Journal*, Vol. 31, No. 7, 1993, pp. 1177–1186.

[10]Kuo, C. H., and Lu, N. Y., "Vortex Characteristics over Delta-Wing Subject to Transient Along-Core Blowing," *AIAA Journal*, Vol. 13, No. 12, 1995, pp. 2418–2420.

[11]Kuo, C. H., and Lin, D. C., "Non-Uniform Recovery of Vortex Breakdown over Delta-Wing in Response to Blowing Along Vortex Core," *Experiments in Fluids*, Vol. 22, No. 1, 1996, pp. 33–44.

[12]Faler, J. H., and Leibovich, S., "Disrupted States of Vortex Flow and Vortex Breakdown," *Physics of Fluid*, Vol. 2, No. 9, 1977, pp. 1385–1400.

[13]Lessen, M., Singh, P. J., and Paillet, F., "The Stability of a Trailing Line Vortex, Part I: Inviscid Theory," *Journal of Fluid*, Vol. 63, Pt. 4, 1974, pp. 753–763.

[14]Howard, L. N., and Gupta, A. S., "On the Hydrodynamics and Hydromagnetic Stability of Swirling Flows," *Journal of Fluid Mechanics*, Vol. 14, Pt. 3, 1962, pp. 463–477.

[15]Robinson, B. A., Barnett, R. M., and Agrawal, S., "Simple Numerical Criterion for Vortex Breakdown," *AIAA Journal*, Vol. 32, No. 1, 1994, pp. 116–122.

[16]Roos, F. W., and Kegelman, J. T., "An Experimental Investigation of Sweep Angle Influence on Delta-wing Flows," AIAA Paper 90-0383, Jan. 1990.

[17]Greenwell, D. J., and Wood, N. J., "Determination of Vortex Burst Location on Delta-Wings from Surface Pressure Measurements," *AIAA Journal*, Vol. 30, No. 11, 1992, pp. 2736–2739.

A. Plotkin
Associate Editor